Strain rate effect on the mechanical properties of a glass fibre reinforced acrylic matrix laminate. An experimental approach

Lucien Cadieu, Jean-Benoit Kopp, Julien Jumel, Jéremy Bega, Catherine Froustey

Strain rate effect on the mechanical properties of a glass fibre reinforced acrylic matrix laminate. An experimental approach

L. Cadieu[a,*], J.B. Kopp[b], J. Jumel[a], J. Bega[b], C. Froustey[a]

[a] Université de Bordeaux, I2M, UMR CNRS 5295, F-33405 Talence, France
[b] Arts et Métiers ParisTech, I2M, UMR CNRS 5295, F-33405 Talence, France

Keywords:
Indentation
Impact
Strain rate
Composite
Laminate
Thermoplastic

A B S T R A C T

The aim of this study is to evaluate the effect of the loading rate on the mechanical properties and damage mechanisms of a Glass/Elium150 laminate composite. Quasi-static indentation (QS) and low energy dynamic impact (DYN) tests which simulate lifetime structural loadings (dropped tool, gravel impacts, …) are lead. A specific experimental approach is developed to compare results of both experiments. The effect of the loading rate on the structural response (stiffness, dissipated energy) of the composite is highlighted. The numerous damage mechanisms involved in the collapse of the material are observed at a microscopic scale using both optical and scanning electron microscopy (SEM). Finally an intra-laminar crack propagation mechanism is described based on post-mortem observations at ply scale to explain the formation of interlaminar cracks.

1. Introduction

A new composite material composed of an acrylic thermoplastic matrix (Elium150) is developed as an alternative to non-recyclable thermosetting composites. Low velocity impact on composite laminates appear in the 1980s and it was observed that the main governor parameter is the impact energy [1]. Since then composite materials have been widely studied under impact loadings thanks experimental approaches [2] or numerically [3,4]. These polymer materials exhibit strong sensitivity of their mechanical properties to temperature and strain rate [5–10]. As expected with a polymeric matrix, the bigger the strain rate, the bigger the elastic modulus and the tensile strength, and the lower the maximum strain [5]. Most of the results published on the strain rate effect on composite materials behaviour are comparable to the bulk polymer behaviour. Some of the observations and results on composites materials are nevertheless contradictory [11]: Armenakas and Sciamarella [12] highlight for example that the ultimate tensile strain and stress of a Glass/Epoxy composite decreased with the loading rate whereas Staab [13] showed that they increased with increasing loading rate. The structural response of the composites is highly dependent on the micro-structure of the material and the interface between both components [14]. The manufacturing and the curing processes as well as the handling often induce intrinsic defects (porosity, micro-cracks, delamination) [15–17] which could affect the structural response of the composites. As suggested by Jacob et al. [11] it is needed to investigate and characterize in detail the strain rate effects on the tensile, compressive, shear, and other mechanical properties of composite materials and a multiscale analysis of damage and fracture mechanisms is necessary to precisely describe the composite behaviour. On the one hand it is known that specific damages such as fibre failure and delamination lead to the collapse of composite structures. On the other hand damage and fracture kinetics is not well known since a precise spatial and temporal damage mechanisms description is necessary. Indeed matrix cracks appear fastly and often at micro-scale. In acrylic matrix for example it is known that crack propagates at several hundred meters per second [18,19]. Generally post-mortem analysis are lead to identify damage mechanisms during dynamic loadings [20–22]. In-situ observations are current to measure strain fields during mechanical loadings but infrequent to describe damage and fracture mechanisms since it depends strongly on technical equipments. Dynamic effects induced by the structural loadings and cracks propagation are limiting. The aim of this paper is to study the load rate effect on mechanical properties of a Glass/Elium150 laminated composite. Indentations and impact tests are lead to compare the quasi-static (QS) and dynamic (DYN) test, test conditions are selected to cover the service impact loading conditions that the laminate may encounter (hail, dropped tool, stone or gravel impacts). At first the tested material is introduced and the experimental methodology is detailed. Then typical responses of the composite to QS and DYN indentations are presented and the differences are highlighted. Subsequently the effect of the

* Corresponding author.
E-mail address: lucien.cadieu@u-bordeaux.fr (L. Cadieu).

https://doi.org/10.1016/j.compstruct.2019.110952

loading rate on the indentation stiffness, the maximum load and the indentation depth of the composite is described. Finally post-mortem observations with optical and scanning electron microscope are lead to describe the damage and fracture mechanisms at microscopic scale and explain the differences between QS and DYN behaviour.

2. Experimental setup and methods

2.1. Material

The tested material are laminate samples manufactured by ARKEMA. They are composed of a polymethylmethacrylate (PMMA-ELIUM 150) resin reinforced with long woven glass fibres (Chomarat G-wave 600P/A). The matrix has a tensile strength of 76 MPa, a tensile modulus of $E = 3300$ MPa and a tensile strain $\varepsilon_m = 6\%$. Samples are infused under room temperature conditions and at atmospheric pressure (500 mbar) and are provided as 100×100 mm^2 plate specimens. Four plies of woven glass fibres are stacked and result in a thickness of 2 mm. Knowing that the laminate matrix is a thermoplastic polymer which is strain rate dependant by nature, the visco-elastic behaviour of the material must be evaluated. Three point bending creep tests are performed on a Dynamic Mechanical Analysis (DMA) machine under room temperature condition (23 °C). Creep tests show that deformation is less than 1% for a 20 min test (Fig. 1). Since the longest indentation test lasts 10 min the visco-elastic deformation can be neglected.

2.2. Experimental setup

2.2.1. Loading and boundary conditions

During both QS and DYN tests the square samples are constrained between two steel clamps that have a circular hole of 85 mm in their center (see in Fig. 2). The steel tip used has a 25 mm diameter hemispherical head. These parameters are selected in order to respect the tip diameter to circular hole diameter ratio of 0.3 recommended in the ASTM D5628-96 test method [23].

2.2.2. Quasi-static tests

The QS tests have been conducted on a universal electromechanical tensile/compression testing machine (Zwick Roell Z250). The cross head displacement and the load are measured during the tests via the crosshead travel encoder (maximal error of ± 0.05% on the displacement and ± 0.08% on the crosshead velocity) of the testing machine and a piezoelectric Kistler load sensor of 10 kN ± 0.25%. The data are recorded at a sampling rate of 100 Hz.

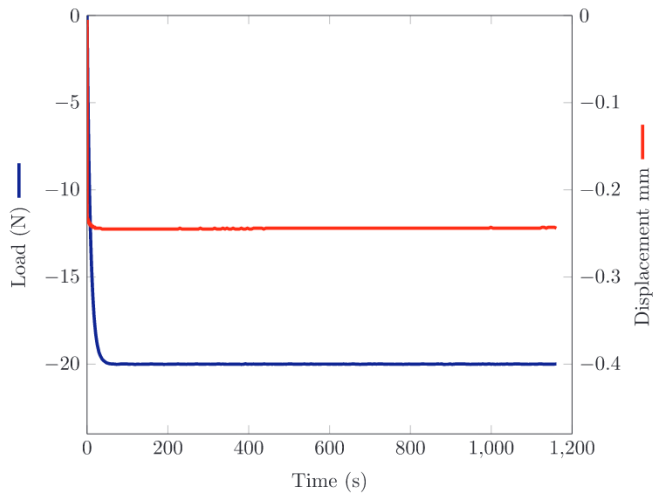

Fig. 1. Verification that the sample relaxation is negligible during the applied loadings.

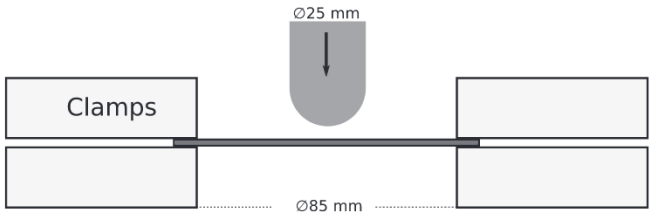

Fig. 2. Clamping system for the experiments.

2.2.3. Dynamic tests

DYN tests are conducted on a vertical drop tower [24,25]. A mass coupled with a 60 kN piezoelectric Kistler load sensor with a sampling rate of 60 kHz is dropped from a specific height giving a theoretical impact velocity ranging from 2 to a maximum of 7 m s^{-1}. The impact energies depend on the mass and the velocity of the impactor. The impactor has a minimum mass of 1.4 kg and the lowest possible velocity is linked to the minimum drop height. The impact energy can be theoretically calculated with the consideration that there is no friction between the drop tower guides and dropped chariot using the relation – $E = 1/2mv^2$. The displacement of the impactor can be measured using a target tracking technique with a high velocity camera (Photron SA5 at a sampling rate of 60 kHz) leading to the experimental impact velocity.

2.3. Strategy

2.3.1. QS and DYN link

In order to evaluate the load rate effects firstly in QS and secondly between QS and DYN tests, specific experimental parameters (indentation depth and loading velocity) have been fixed. In the QS campaign each test has its specific depth-load rate couple and during all the tests the same data are measured: the load during the indentation and the displacement of the impactor. The load-displacement curve is integrated to access to the indentation energies: E_{max} the maximum applied energy, $E_{ela.}$ the elastic energy released by the sample and $E_{dis} = E_{max} - E_{ela.}$ the dissipated energy. E_{max} in QS is calculated using the load-displacement measurements. Fig. 3 explains how the different energies, the stiffness K (defined as the slope of the load-displacement curve after the foot slope and before the onset of the first material damages and is given in N mm^{-1}), the maximum indentation depth

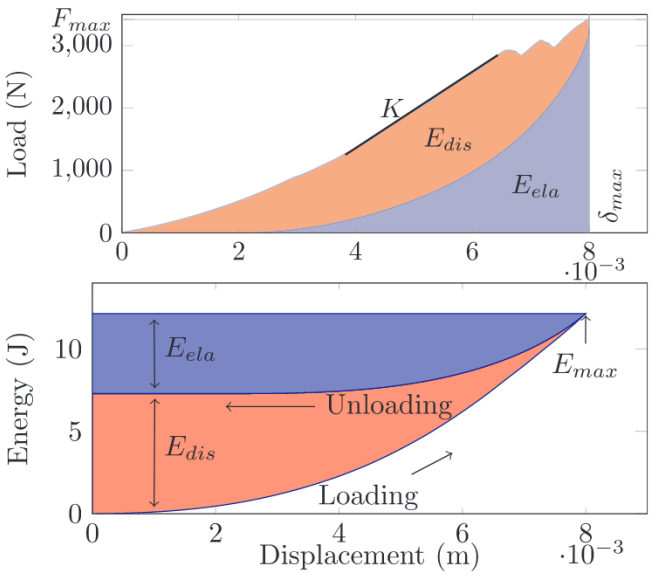

Fig. 3. Determination of the elastic energy and the dissipated energy on both load-displacement and energy displacement curves. The elastic energy is defined by $E_{diss} = E_{max} - E_{ela}$.

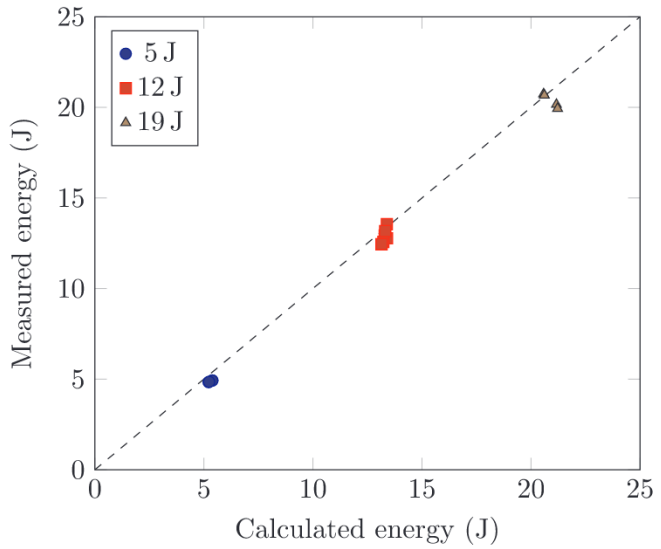

Fig. 4. Comparing the measured energy using $\int_0^{\delta} F d\alpha$ and calculated energies $E = \frac{1}{2}mv^2$ of the DYN tests.

δ_{max} and the maximum load F_{max} are measured. In the DYN campaign each test will have a specific impact energy and loading velocity. The measured data are the tip displacement and the load meaning that the impact energy can be calculated as in the QS campaign. As expected (see in Fig. 4) the theoretically applied energy ($1/2\,mv^2$) is approximatively equal to the measured applied impact energy.

The QS indentation energy is calculated for each QS test and is then applied in the DYN campaign. Therefore the samples are tested at different velocities but with an identical loading energy. This is a key point in order to compare QS and DYN tests. If the applied energy is the same but at different velocities then some results (the measured load, the maximum tip displacement and the damage mechanisms) might show strain rate effects. The parameters are mapped out in Table 1.

2.3.2. Quasi-static tests

As reported in ([26]), one can identify three kinds of step loading: rebound, penetration and perforation. For a rebound step loading, a part of the indentation energy is released elastically by the sample after unloading. When the indention energy equals the dissipated energy, a step penetration loading is reached. A perforation step loading is considered once the indenter breaks through the sample. In this study only rebound and penetration tests are lead in order to study the damage. Indeed if the indenter perforates the sample it must be pulled out which can further damage the samples. After calibration tests, the minimum and maximum indentation depths have been set at 6 and 10 mm. The first damage can be "heard" at 6 mm and the sample is penetrated at 10 mm. Fibre breaking can be heard when the sample is penetrated past the minimum penetration depth which induced the first load drop on the load-displacement curves. The minimum and maximum indenter velocities are selected in order to range over two decades (Table 2). An experimental design of experiments (Doelhert [25,27,28]) is defined to optimize the testing parameters in order to obtain response surfaces

Table 1
Experimental parameters (applied and measured) during QS and DYN experiments.

QS		DYN	
Applied Parameters	Measured data	Applied Parameters	Measured data
v ($\mathrm{m\,s^{-1}}$)	F (N)	E (J)	F (N)
δ (m)			δ (m)

Table 2
Definition of the measured indentation and impact velocities ($\mathrm{m\,s^{-1}}$). $v1$–$v3$ are the QS velocities and $v4$ is the DYN velocity used in the experimental campaigns.

	$v1$	$v2$	$v3$	$v4$
QS	1.6×10^{-5}	8.4×10^{-4}	1.6×10^{-3}	
DYN				2.50

N	X_1	X_2	X_3
1	0.000	0.000	0.000
2	1.000	0.000	0.000
3	-1.000	0.000	0.000
4	0.500	0.866	0.000
5	-0.500	-0.866	0.000
6	0.500	-0.866	0.000
7	-0.500	0.866	0.000
8	0.500	0.289	0.816
9	-0.500	-0.289	-0.816
10	0.500	-0.289	-0.816
11	0.000	0.577	-0.816
12	-0.500	0.289	0.816
13	0.000	-0.577	0.816

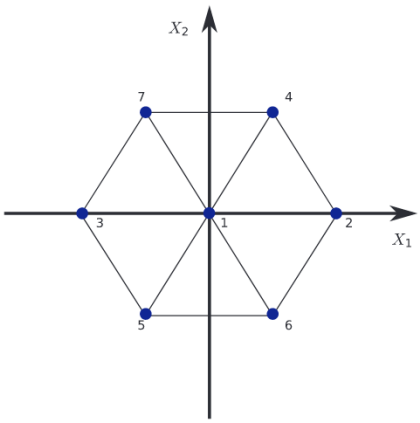

Fig. 5. Doelhert matrix for two and three variables. Two variable experimental design. N is the number of the experiment, X_1 and X_2 are the coded variables.

with a minimum number of experiments. The response surfaces are modelled with a second order polynomial (Eq. (1)) where X_1 and X_2 are coded variables. The experimental design is plotted and the coded variables are given in Fig. 5 with X_1 the depth and X_2 the velocity.

$$y = a_0 + a_1X_1 + a_2X_2 + a_{11}X_1^2 + a_{22}X_2^2 + a_{12}X_1X_2 \quad (1)$$

The QS response surfaces will plot the maximum load withstood by the sample and the damages area (DA) against the indentation depth and velocity.

2.3.3. Drop tower tests

In order to apply the energy determined in the QS loadings the velocities are limited to 2–3 $\mathrm{m\,s^{-1}}$ so an average speed of 2.5 $\mathrm{m\,s^{-1}}$ is selected. No mass influence can be observed for low energy impacts [29]. Therefore the mass will vary in order to apply the necessary energies for DYN indentation tests. Only one decade of $\dot{\delta}$ is reachable during the drop tower campaign. An experimental design is therefore not necessary.

2.4. Damage observation

The damaged area (DA) is estimated using the transparency of the samples by placing a light beneath the samples [30]. This technique is possible since the samples are translucent. The damages deviate and stop the light from going through the sample which makes the damaged area darker when looking from above. The damaged area is directly estimated and measured with the help of a Keyence vhx-1000 optical microscope. These observation only give a projected damaged area since it is known that the damage occurs through out the thickness and can have different profiles [31,32].

A scanning electron microscope using backscatter electrons (SEM-BSE) is also used to observe damage mechanisms that occur at different scales. The sample (i.e. the plate) is first sawed on the outskirts of the damaged area. It is then coated with a PMMA resin to avoid further damaging the material when accessing the center of the DA (see in Fig. 6). Indeed the sample is cut using a vertical cut-off saw close to the center of indentation area perpendicularly to the indented surface. The samples are then polished using sand papers ranging from a P800 to

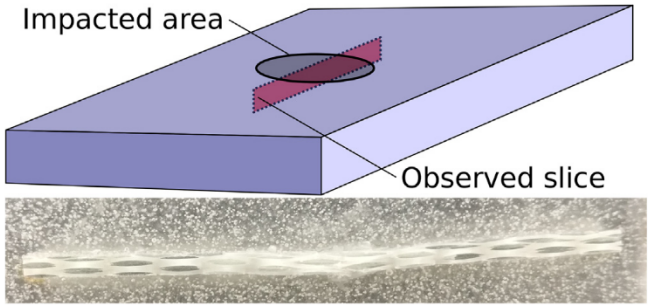

Fig. 6. Observed slice of the sample under SEM-BSE before metallisation. The bottom image shows the observed slice trapped in polymer (area with bubbles) before metallization.

Table 3
Experimental parameters and results for QS tests. The measurement uncertainty is linked to the instruments used. These uncertainties are propagated to the calculated data.

Sample ID	δ_{maxQS} [mm] ±0.05%	F_{maxQS} [N] ± 0.25%	K [N mm^{-1}] ± 2.7%	E_{maxQS} [J] ± 0.7%	E_{elaQS} [J] ± 0.7%	E_{dissQS} [J] ± 0.7%	DA [mm^2]
D6v2	6	2480	498	5.9	3.48	2.42	47
D7v1	7	2410	422	7.3	3.34	3.96	68
D7v3	7	3100	500	8.9	4.6	4.3	48
D8v2_1	8	3420	503	12.2	4.86	7.34	132
D8v2_2	8	3340	530	12.5	4.54	7.96	115
D8v2_3	8	3320	485	12.2	4.99	7.21	106
D9v1	9	2650	414	12.1	3.08	9.02	175
D9v3	9	3760	491	15.5	4.07	11.43	171
D10v2	10	3830	480	17.7	4.07	13.63	275

P4000. The observed surface is finally coated with a thin layer of gold (few nm) making it a conducting surface and observable with the SEM.

2.4.1. Sample identification

The QS and DYN velocities are given in Table 2. The samples are referenced by the depth (D) in QS or energy (E) in DYN and the loading velocity (v). For example in the QS experiments, a laminate indented by 8 mm at a velocity of 1.6×10^{-5} m s^{-1} will be named D8v1. A sample named E12_v4_2 is a DYN sample tested at an impact energy of 12 J, at a velocity identified of 2.5 m s^{-1} and is the second test in these conditions.

3. Results

The contact force, the elastic energy returned and the dissipated energy were determined for each experiment in both QS and DYN tests. The QS and DYN experimental parameters and results are respectively given in Tables 3 and 4 for each specimen. Additionally, to compare QS and DYN for a given maximum energy, the mean value of all the data are reported in Table 5.

3.1. Load-displacement

The load vs time evolution was recorded for each test. It can be seen in Tables 3 and 4 that the experiments are reproducible. Indeed, under the same experimental conditions, less than 5% dispersion is achieved on F_{max}.

Influence of the loading rate is evident in the QS tests results presented in Fig. 7. The load vs displacements curves have been plotted for 7 and 9 mm indentation values and $v1$ and $v3$ indentation rate values. The first damage is observed for indentation depth values between 8 and 9 mm. Indeed past this critical indentation depth (δ_c) the sample visible cannot sustain higher load. The load is sufficient to onset internal material damage such as fibre or ply failure or delamination [33]. The maximum load measured for a 7 mm indentation at $v1$ is 2410 N and rises to 3100 N for $v3$ showing a 28% increase. For a 9 mm indentation depth the maximum load increase reaches 40%. This is directly linked to the increase of the sample stiffness when the load rate increases. During the QS tests the stiffness increases by 20% when the velocity increases from $v1$ to $v3$. It can also be seen when plotting the response surfaces linked to the experimental design in Fig. 8–10.

DYN and QS results are then compared for the same 12 J applied energy (see Fig. 11). The maximum load clearly increases while the maximum displacement decreases when the load rate increases. The maximum load increases by 35%. When comparing QS and DYN tests the stiffness continues to increase with the loading velocity. Indeed for a 12 J QS indentation the sample stiffness is of 506 N mm^{-1} and for a 12 J DYN indentation the stiffness is of 883 N mm^{-1}. In average the stiffness increases by 75% (Table 5). Furthermore the indentation depth seems to lower as the load rate increases as can be seen in Fig. 11.

3.2. Elastic and dissipated energies

The elastic energy under DYN loadings is higher than under QS loadings as can be seen in Fig. 12. The elastic energy stored in the specimen under QS loading seems to be insensitive to the applied energy. For DYN loadings the elastic energy increases with the applied energy.

Table 4
Experimental parameters and results for DYN tests.

Sample ID	E_{maxDYN} [J]	δ_{maxDYN} [mm]	F_{maxDYN} [N]	K [N mm^{-1}]	E_{elaDYN} [J]	$E_{dissDYN}$ [J]	DA [mm^2]
E5_v4_1	4.93	5.07	2498	835	3.62	1.31	44
E5_v4_2	4.92	4.95	2520	804	3.43	1.49	51
E5_v4_3	4.83	4.89	2410	767	3.36	1.47	47
E5_v4_4	4.85	4.70	2599	845	3.37	1.48	43
E12_v4_1	12.93	7.69	4430	891	7.73	5.20	142
E12_v4_2	12.77	7.08	4606	854	7.68	5.09	134
E12_v4_3	12.58	7.23	4582	916	7.46	5.12	95
E12_v4_4	12.44	7.23	4407	917	6.26	6.18	106
E12_v4_5	13.55	7.59	4726	828	8.94	4.61	114
E12_v4_6	13.17	7.17	4530	893	6.98	6.19	109
E19_v4_1	20.16	8.30	5815	932	9.18	10.98	159
E19_v4_2	19.94	8.31	5891	937	7.90	12.04	150
E19_v4_3	20.74	8.51	6233	926	10.1	10.64	117
E19_v4_4	20.67	8.65	6210	834	10.2	10.47	121

Table 5
Averaged summarised data of QS and DYN tests.

E_{max} (J)	K_{max} (N mm^{-1})		F_{max} (N)		δ (mm)		E_{ela} (J)		E_{dtss} (J)		DA (mm^2)	
	QS	DYN	QS	DYN	QS	DYN	QS	DYN	QS	DYN	QS	DYN
5–6	498	813	2480	2510	6	5	3.5	3.5	2.5	1	47	46
12	506	883	3360	4546	8	7.3	4.8	7.5	7.5	5.4	118	117
18–20	480	907	3830	6037	10	8.4	4.07	9.3	13.63	11	275	137

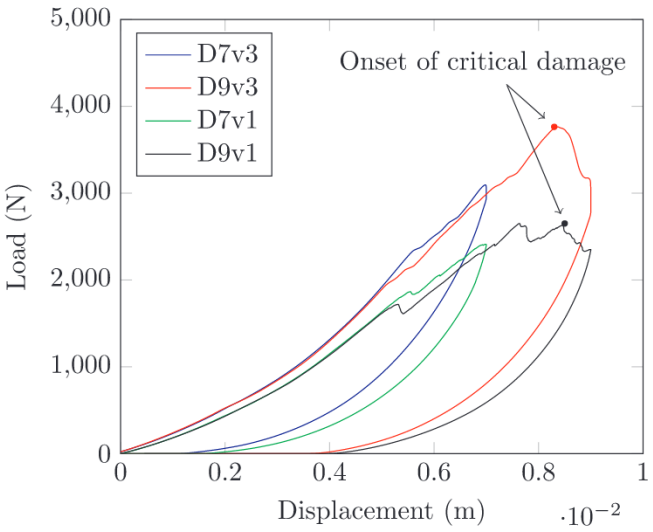

Fig. 7. $F(\delta)$ curves for speeds of 1.6×10^{-5} m s^{-1} and 1.6×10^{-3} m s^{-1}.

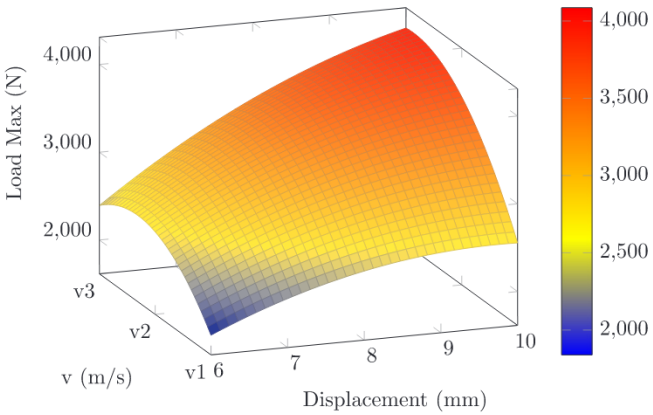

Fig. 8. $F(\delta, v)$ answer surface linked to the experimental design of Doelhert for the QS campaign.

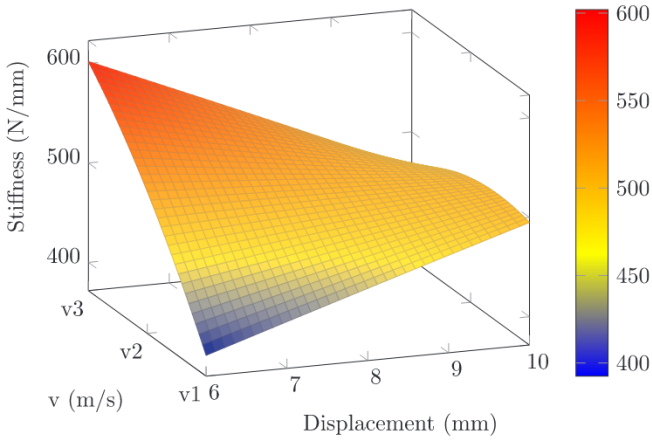

Fig. 9. $K(\delta, v)$ answer surface linked to the experimental design of Doelhert for the QS campaign.

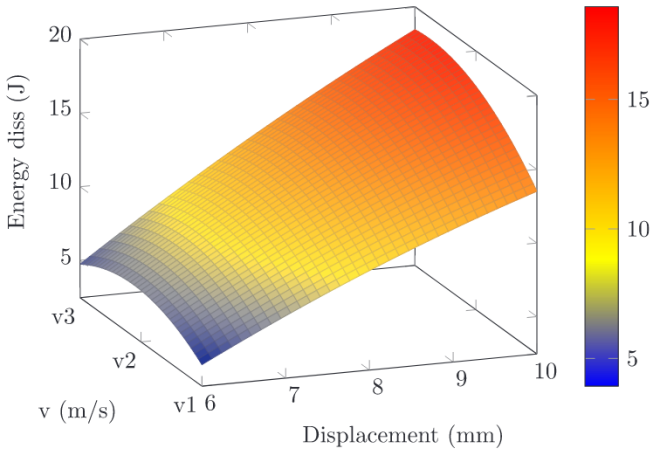

Fig. 10. $E(\delta, v)$ answer surface linked to the experimental design of Doelhert for the QS campaign.

When observing E_{elaQS} in Table 5 it seems that this parameter is independent on the loading depth and velocity. It has an approximately constant value of 4.1 ± 0.7 J for all the experiments. As the applied energy increases only the dissipated energy increases. Different results are observed under DYN loading. As long as the impactor rebounds off the sample E_{elaDYN} seems dependent to the applied energy. Indeed under DYN loading it seems the bigger the applied energy the bigger the value of E_{elaDYN}. When 5 J impact energy was applied E_{elaDYN} is 3.45 ± 0.12 J, for 12 J E_{elaDYN} is 7.76 ± 0.72 J and for 19 J E_{elaDYN} is 9.35 ± 1.07 J. Unlike the QS experiments were E_{elaQS} is roughly the same for all applied energies E_{elaDYN} is clearly linked to the applied energy.

3.3. Damaged area (DA)

It has been shown that as E_{max} increases E_{dis} increases in both QS and DYN tests. One can expect to observe larger damaged zones in the specimen as E_{dis} increases or a higher density of cracks, voids under the impact zone. So for the same applied energy in QS and DYN tests E_{disQS} is higher than E_{disDYN}. As a consequence the damage under QS and DYN loadings should be different in nature and quantitatively.

It can be seen in Table 5 that the DA increases with increasing E_{dis} and δ. The DA seems to be more sensitive to δ than to E_{dis}. Indeed past δ_c ($8 \leqslant \delta_c \leqslant 9$ mm) the DA seems to skyrocket. For all applied energies the measured E_{dis} in QS and DYN experiments are roughly the same yet for 19 J the QS DA is nearly twice as big as the DYN DA. It can possibly be explained by the 19 J indentation depth: $\delta_{DYN} < \delta_c < \delta_{QS}$. The damaged area is more driven by the penetration depth than the impact enegy. Before the critical indentation depth, DA are quite identical between QS and DYN sollicitations. It shall be assumed that the difference in impact energy can be neglected comparatively to a penetration depth difference.

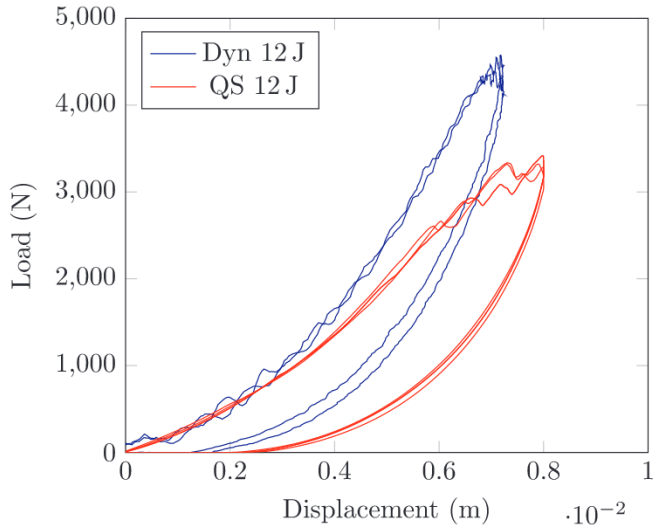

Fig. 11. $F(\delta)$ curves for QS and DYN curves. The applied energy is 12 J. It is visible that the maximum load is higher for a DYN loading than a QS loading. δ_{DYN} is lower than δ_{QS} since the tests are lead at iso-energy.

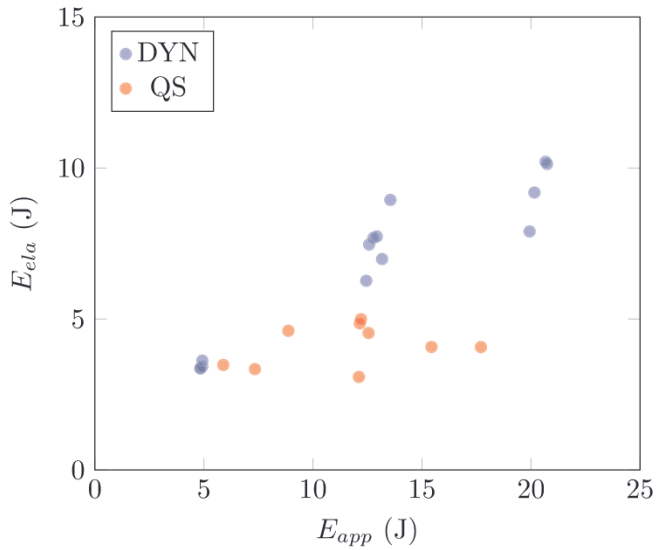

Fig. 12. Elastic energy versus the applied energy for both QS and DYN tests. The QS elastic energy seems to be insensitive to the applied energy whereas the DYN elastic energy seems to be sensitive to the applied energy.

3.4. SEM observations and damage mechanisms

Damage mechanisms are investigated using an electron microscope observations. Classical damages such as matrix cracking, fibre/matrix de-cohesion, fibre failure, strand failure and ply failure can be clearly identified. All tested samples have been observed. At macro-scale (i.e. the laminate scale) the primary damage mechanisms that have been identified right below the impactor are: ply failure, strand failure, matrix fracture and delamination (see in Fig. 13). Note that a defect (porosity) has also been identified in Fig. 13. As expected the area right bellow the impactor is more damaged. The major visible damages outside the impacted area are matrix fracture, fibre-matrix de-cohesion and delamination. At meso-scale (i.e. the ply scale) the primary damage mechanisms are strand failure, fibre failure and matrix fracture as seen in Fig. 14. One can also see two micro-damage mechanisms in Fig. 14: in the circle areas broken fibres are shown, in the square areas fibre-matrix de-cohesion can be seen for both 0 and 90° orientations. The

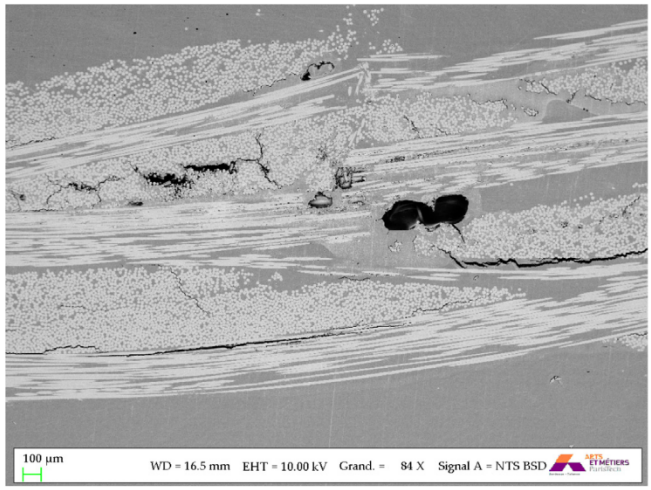

Fig. 13. SEM-BSE observation of damages in sample $d7v1$. Strands are clearly visible and have a white color, the matrix is visible and has a grey coclor, an initial defect and the damages are black.

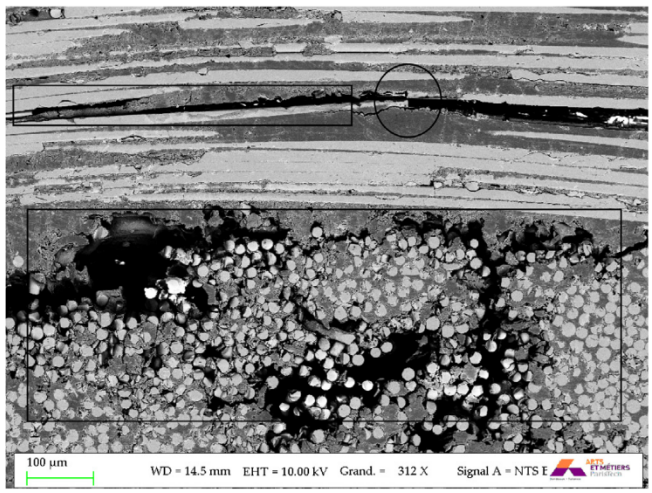

Fig. 14. Two visible damages identified in sample $d9v1$. Fibre–matrix de-cohesion can be seen in the square areas for both fibre orientations. Fibre failure can be seen in the circle area.

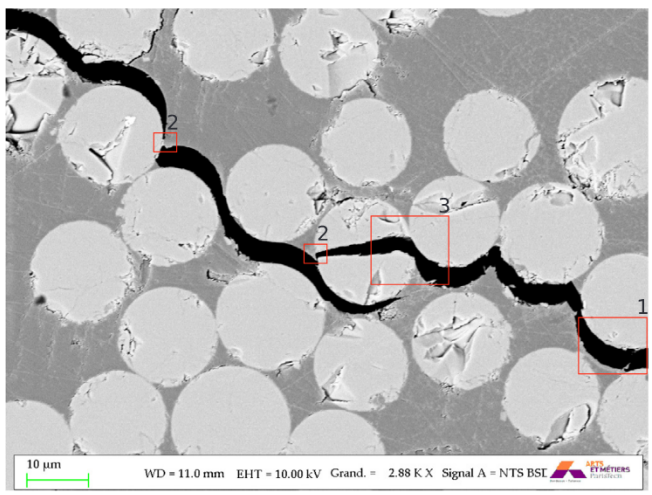

Fig. 15. Crack propagation path in a strand of sample $d8v6$. It can be seen that the micro-cracks (2) favors the fibre–matrix interface to propagate (1). When two fibres are in contact the crack will break the second fibre (3).

fibres in the bottom square have no matrix on their surface. This shows that the fibre-matrix interface is more brittle than the matrix itself. This result is supported by the crack propagation path seen in the samples and observed in Fig. 15. The crack propagates mainly in the fibre–matrix interface. Nevertheless it seems that when the crack is confined between two fibres the second fibre on the crack path breaks. This mechanism has been observed for all applied energies and velocities. Post-mortem SEM analyses do not reveal a load rate effect on damage mechanisms. Indeed they are all observable whatever the loading rate (QS or DYN).

4. Discussion and conclusion

This study aims to evaluate the mechanical response of thermoplastic composite plates under various indentation rate conditions. As expected for polymeric materials rate dependence is observed at macroscopic scale. As generally observed, the higher the loading rate, the larger the Young's modulus value, the higher the maximum stress and the lower the failure strain. Two types of mechanical tests have been performed to vary the loading rate condition and the loading intensity corresponding to quasi-static indentation (10^{-5}–10^{-3} ms^{-1}) and low energy impact (2.5 ms^{-1}). It has been observed that the bigger the loading rate (i.e. the indentation/impact velocity), the bigger the stiffness K, the bigger the maximum load F_{max} and the lower the penetration depth δ_{max}. This confirms at this scale the loading rate dependence on the mechanical response of this composite laminate. Elastic and dissipated energies have been estimated by integration of the load-displacement curve. As expected it has been observed that these energies are significantly dependent on the applied energy and therefore the penetration depth. The bigger the loading rate, the lower the penetration depth, the lower the dissipated energy and the bigger the elastic energy. The damaged area (DA) which gives a 2D information on the extent of damage is measured by visual inspection. Before a critical depth δ_c it seems that the DA is approximately identical in both QS and DYN and is limited to the region bellow the indenter. After this critical value, the DA skyrockets. In QS between 8 and 10 mm penetration depth values, the DA more than doubles in size (117 ± 14 mm^2 to 275 mm^2). Damaged mechanisms have been also investigated post-mortem with SEM observations. Whatever the loading rate all "classical" damages observed in a thermoplastic composite plate have been identified. Delamination, matrix fracture and fibre failure are predominant. Micro-cracks are observed at component scale. This kind of mechanism is known to be loading rate sensitive. It is indeed known that for acrylic resins (an amorphous polymer), the higher the energy input, the faster and the longer the cracks propagate. The use of a SEM to perform post-mortem analyses limits the finding of differences if they exist.

Whatever the 2D analysis method, with the damaged area and damage mechanisms observed respectively at the surface and in the width of the sample with the SEM, the loading rate seems to be a second order parameter. These mechanisms seem to be finally more driven by the penetration depth than the loading rate. Post-mortem 2D analyses can not give information on the damaged volume nor on the damage kinetic. In-situ micro-tomography analyses should be relevant in order to capture these informations and highlight if it exists a loading rate effect on the damage mechanisms appearance. The effect of rapid loading and faster energy delivery could probably have an influence on the kinetics of occurrence of damage and potentially the propagation of cracks.

Finally one can conclude that:

- The loading rate has a significant influence on the macroscopic parameters (F_{max}, K, δ) of the behaviour of the sample.
- The loading rate seems to be a second order parameter on damage mechanisms which have been observed post-mortem with SEM analyses.
- In-situ analyses are necessary to access to the kinetic of damage mechanics appearance which are probably different as a function of the loading rate.

Acknowledgement

The authors gratefully acknowledge ARKEMA for providing the samples and especially P. Gerard for the meaningful scientific discussions.

References

[1] Caprino G, Crivelli Visconti I, Di Ilio A. Composite materials response under low-velocity impact. Compos Struct 1984;2:261–71.
[2] Atas C, Sayman O. An overall view on impact response of woven fabric composite plates. Compos Struct 2008;82(3):336–45.
[3] Kinvi-Dossou G, Matadi Boumbimba R, Bonfoh N, Koutsawa Y, Eccli D, Gerard P. A numerical homogenization of E-glass/ acrylic woven composite laminates: application to low velocity impact. Compos Struct 2018;200:540–54.
[4] Boufaida Z, Boisse J, André S, Farge L. Mesoscopic strain field analysis in a woven composite using a spectral solver and 3D-DIC measurements. Compos Struct 2017;160:604–12.
[5] Halary LMJL, Laupretre F. Mécanique des matériaux polymères. Belin 2008.
[6] Richeton J, Ahzi S, Vecchio K, Jiang F, Adharapurapu R. Influence of temperature and strain rate on the mechanical behavior of three amorphous polymers: characterization and modeling of the compressive yield stress. Int J Solids Struct 2006;43(7–8):2318–35.
[7] Vieille B, Aucher J, Taleb L. Influence of temperature on the behavior of carbon fiber fabrics reinforced PPS laminates. Mater Sci Eng: A 2009;517(1–2):51–60.
[8] Vieille B, Taleb L. About the influence of temperature and matrix ductility on the behavior of carbon woven-ply PPS or epoxy laminates: notched and unnotched laminates. Compos Sci Technol 2011;71(7):998–1007.
[9] Hassan A, Haworth B. Impact properties of acrylate rubber-modified PVC: influence of temperature. J Mater Process Technol 2006;172(3):341–5.
[10] Zabala H, Aretxabaleta L, Castillo G, Aurrekoetxea J. Loading rate dependency on mode I interlaminar fracture toughness of unidirectional and woven carbon fibre epoxy composites. Compos Struct 2015;121:75–82.
[11] Jacob G, Starbuck J, Fellers J, Simunovic S, Boeman R. Strain rate effects on the mechanical properties of polymer composite materials. J Appl Polym Sci 2004;94(1):296–301.
[12] Sciammarella CA, Armenàkas AE. Response of glass-fiber-reinforced epoxy specimens to high rates of tensile loading. Exp Mech 1973:433–40.
[13] Staab G, Gilat A. High strain rate response of angle-ply glass/epoxy laminates. J Compos Mater 1995;29(10):1308–13.
[14] Boufaida Z, Farge L, André S, Meshaka Y. Influence of the fiber/ matrix strength on the mechanical properties of a glass fiber/ thermoplastic-matrix plain weave fabric composite. Compos Part A: Appl Sci Manuf 2015;75:28–38.
[15] Bolotin V. Delaminations in composite structures: its origin, buckling, growth and stability. Compos Part B 1996;27B(95):129–45.
[16] Bolotin V. Mechanics of delamination in laminate composite structures. Mech Compos Mater 2001;37:367–80.
[17] Tay T, Shen F. Analysis of delamination growth in laminated composites with consideration for residual thermal stress effects. J Compos Mater 2002;36(11):1299–320.
[18] Kopp JB, Schmittbuhl J, Noel O, Lin J, Fond C. Fluctuations of the dynamic fracture energy values related to the amount of created fracture surface. Eng Fracture Mech 2014;126:178–89.
[19] Kopp JB, Schmittbuhl J, Noel O, Fond C. A self-affine geometrical model of dynamic RT-PMMA fractures: implications for fracture energy measurements. Int J Fracture 2015;193(2):141–52.
[20] Dehkordi MT, Nosraty H, Shokrieh MM, Minak G, Ghelli D. Low velocity impact properties of intra-ply hybrid composites based on basalt and nylon woven fabrics. Mater Des 2010;31(8):3835–44.
[21] Bandaru AK, Patel S, Ahmad S, Bhatnagar N. An experimental and numerical investigation on the low velocity impact response of thermoplastic hybrid composites. J Compos Mater 2017:1–13.
[22] Matadi Boumbimba R, Coulibaly M, Khabouchi A, Kinvi-Dossou G, Bonfoh N, Gerard P. Glass fibres reinforced acrylic thermoplastic resin-based tri-block copolymers composites: low velocity impact response at various temperatures. Compos Struct 2018;160:939–51. (November 2016).
[23] ASTM D 5628-96. Stand Test Method for Impact Resistance of Flat Rigid Plastic Specimens by Means of a Falling Dart (Tup or Falling Mass).
[24] Ballère L, Viot P, Guillaumat L, Cloutet S. Damage tolerance of impacted curved panels L. Int J Impact Eng 2009;36:243–53.
[25] Guillaumat L, Baudou F, De Azevedo AMG, Lataillade JL. Contribution of the experimental designs for a probabilistic dimensioning of impacted composites. Int J Impact Eng 2005;31(6):629–41.
[26] Aktaş M, Atas C, Içten B, Karakuzu R. An experimental investigation of the impact response of composite laminates. Compos Struct 2009;87(4):307–13.
[27] Doelhert D. Uniform shell designs. Appl Stat 1970;19(3):231–9.
[28] Doelhert D, Klee V. Experimental designs through level reduction of the d-dimensional cuboctahedron. Discrete Math 1972;2:309–34.
[29] Varas D, Artero-Guerrero J, Pernas-Sánchez J, López-Puente J. Experimental study

of the impactor mass effect on the low velocity impact of carbon/epoxy woven laminates. Compos Struct 2015;133:774–81.
[30] Icten BM. Low temperature effect on single and repeated impact behavior of woven glass-epoxy composite plates. J Compos Mater 2014:1–8.
[31] Caprino G, Carrino L, Durante M, Langella A, Lopresto V. Low impact behaviour of hemp fibre reinforced epoxy composites. Compos Struct 2015;133:892–901.
[32] Shyr T-W, Pan Y-H. Impact resistance and damage characteristics of composite laminates. Compos Struct 2003;62(2):193–203.
[33] Belingardi G, Vadori R. Low velocity impact tests of laminate glass-fiber-epoxy matrix composite material plates. Int J Impact Eng 2002;27(2):213–29.